Tip-Clearance Actuation With Magnetic Bearings for High-Speed Compressor Stall Control

Proceedings of
ASME TURBOEXPO 2000
May 8-11, 2000, Munich Germany

2000-GT-0528

TIP-CLEARANCE ACTUATION WITH MAGNETIC BEARINGS FOR HIGH-SPEED COMPRESSOR STALL CONTROL

Z. S. Spakovszky, J. D. Paduano
Gas Turbine Laboratory
Department of Aeronautics and Astronautics
Massachusetts Institute of Technology
Cambridge, MA 02139

R. Larsonneur, A. Traxler
MECOS Traxler AG
Winterthur, CH 8404
Switzerland

M. M. Bright
NASA Glenn Research Center
Cleveland, OH 44135

ABSTRACT

Magnetic bearings are widely used as active suspension devices in rotating machinery, mainly for active vibration control purposes. The concept of active tip clearance control suggests a new application of magnetic bearings as servo-actuators to stabilize rotating stall in axial compressors.

This paper presents a first-of-a-kind feasibility study of an active stall control experiment with a magnetic bearing servo-actuator in the NASA Glenn high-speed single-stage compressor test facility. Together with CFD and experimental data a two-dimensional, incompressible compressor stability model was used in a stochastic estimation and control analysis to determine the required magnetic bearing performance for compressor stall control. The resulting requirements introduced new challenges to the magnetic bearing actuator design. A magnetic bearing servo-actuator was designed which fulfilled the performance specifications. Control laws were then developed to stabilize the compressor shaft. In a second control loop, a constant gain controller was implemented to stabilize rotating stall. A detailed closed loop simulation at 100% corrected design speed resulted in a 2.3% reduction of stalling mass flow which is comparable to results obtained in the same compressor by Weigl et al. (1998) using unsteady air injection.

The design and simulation results presented here establish the viability of magnetic bearings for stall control in aero-engine high-speed compressors. Furthermore the paper outlines a general design procedure to develop magnetic bearing servo-actuators for high-speed turbomachinery.

1 INTRODUCTION

The stable operation of axial flow compressors, as they are encountered in modern jet engines and gas turbines, is often limited by two flow breakdown processes known as surge and rotating stall. Surge is a circumferentially uniform pulsation of the mass flow through the machine, while rotating stall appears as a reduced flow region in part of the circumference, which travels around the compressor annulus at a fraction of rotor speed. Active control of rotating stall was first proposed by Epstein et al. (1989) and since then a significant amount of further research has been done. In particular theoretical and experimental investigations have been conducted at the NASA Glenn Research Center on a single-stage transonic core compressor inlet stage. Active stabilization of rotating stall and surge using unsteady air injection was first presented by Weigl et al. (1998) in the NASA high-speed stage. The experiments showed a significant benefit

in stable operating range.

Blade tip clearance in axial flow compressors is known to have a strong impact on compressor performance and stability; it also plays a major role in the interaction between rotordynamic shaft deflections and the aerodynamic behavior of the compressor. Graf et al. (1997) report an experimental and analytical investigation of circumferentially non-uniform tip-clearance effects on axial compressor stability and performance. The study reveals that the compressor pre-stall dynamics are very sensitive to the blade tip-clearance. Based on this conceptual framework Gordon (1999) extended this approach to analyze the influence of rotating clearance asymmetries. The work presented here uses a modified version of this compressor model and introduces the concept of tip-clearance actuation for compressor stall control.

Magnetic bearings are widely used as active suspension devices in rotating machinery, mainly for active vibration control purposes. The concept of active tip clearance control suggests a new application of magnetic bearings as servo-actuators to stabilize rotating stall in axial compressors. The magnetic bearing servo-actuator is used to *actively* whirl the shaft inducing an unsteady variation of the rotor blade tip-clearance distribution as shown in Figure 1.

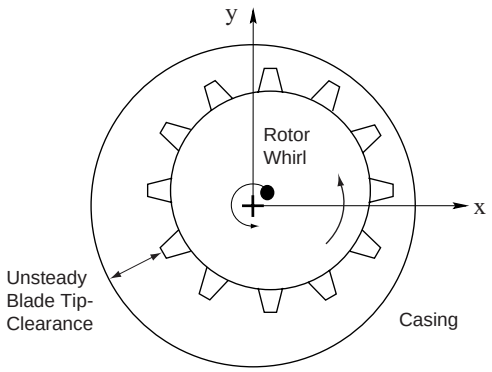

Figure 1. Active tip-clearance stall control concept.

This paper presents a feasibility study and the design of a stall control experiment on a transonic compressor stage. The following research questions are of interest and addressed in this paper:

– How does a magnetic bearing servo-actuator for stall control differ from conventional magnetic levitation devices?

– How much control authority and shaft motion is required to stabilize rotating stall?

– How beneficial is tip-clearance actuation compared to unsteady air injection and other actuation schemes?

– What analytical process has to be conducted in order to design a stall control experiment with magnetic bearings?

The organization of the paper is briefly outlined to guide the reader through the design process. The general sequence of steps involved in the analysis and design of an axial compressor magnetic bearing system is depicted in Figure 2. First, in Section 2,

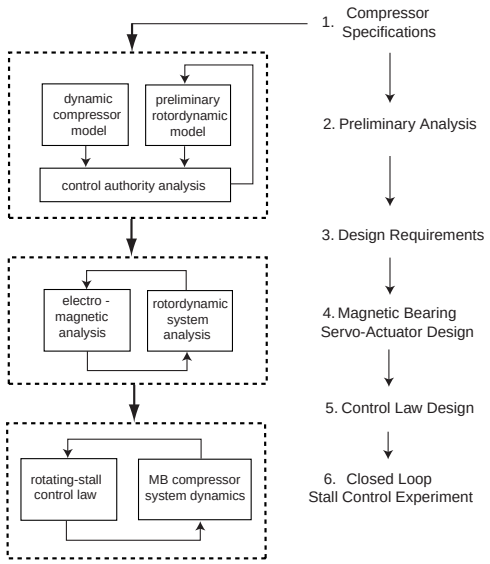

Figure 2. Design process for an axial compressor magnetic bearing system.

the axial flow compressor specifications and the test facility envelope are discussed. Then in Section 3 an unsteady compressor tip-clearance model and a simple, first cut rotordynamic model of the compressor system are implemented in a preliminary analysis to determine the control authority and the design requirements which are discussed in Section 4. The detailed design of the magnetic bearing servo-actuator and rotor system is outlined in Section 5, and the final closed loop system simulation results are presented in Section 6.

The above design process is implemented in an example analysis for the NASA Glenn high-speed single stage axial flow compressor and results specific to this compressor are reported in this paper.

2 AXIAL COMPRESSOR RIG SPECIFICATIONS

The NASA Stage 37 test compressor, originally designed as an inlet stage of an eight-stage 20:1 pressure ratio core compressor (Reid and Moore, 1978a), has a total pressure ratio of 2.05, a mass flow of 20.2 kg/s, a rotor tip speed of 454 m/s, and a rotation frequency of 286 Hz at design conditions. Rotor 37 consists

of 36 blades with an aspect ratio of 1.19, a hub-to-tip radius ratio of 0.7, and a blade tip diameter of approximately 50 cm. The mean-line rotor chord length is 56 mm. Detailed performance descriptions are given by Reid and Moore (1978b).

Atmospheric air is drawn into the test facility through an orifice plate and a plenum chamber upstream of the test section. Downstream of the compressor the flow is regulated with a sleeve-type throttle valve and the compressor shaft is coupled over a drive train to a 2.2 MW DC drive motor. The shaft setup of the test compressor is an over-hung rotor with radial fluid film bearings at the front (near the rotor disk) and at the back of the compressor (near the motor drive coupling) as well as a fluid film thrust bearing on the motor coupling side. A schematic of the test section and the compressor shaft is shown in Figure 3.

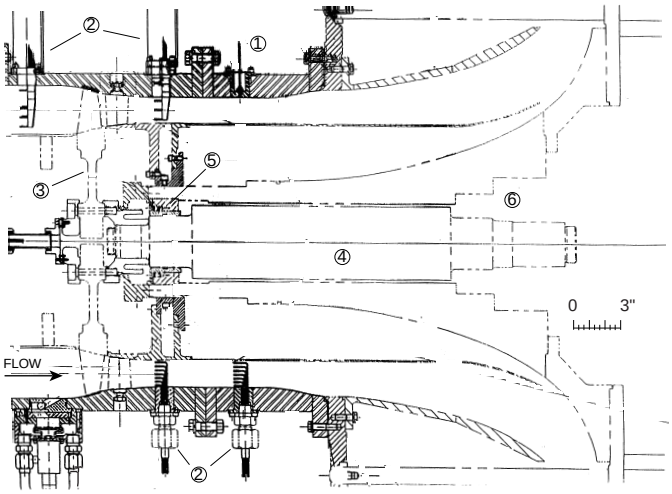

Figure 3. NASA Glenn high-speed single stage compressor test facility.

In this specific case it is desired to limit modifications to the compressor test rig as much as possible. The rear fluid film journal and thrust bearings must be kept the same to mate with the existing motor drive train. The front fluid film journal bearing is to be replaced by the magnetic bearing servo-actuator. Fail-safe operation of the magnetic bearing is compulsory and a special catcher bearing system is to be designed. Also the compressor gas path must remain the same to yield an unchanged aerodynamic compressor performance.

3 PRELIMINARY ANALYSIS

The effect of tip-clearance asymmetries due to shaft deflections on compressor performance and stability is addressed next. The objective of the preliminary analysis is to determine the magnetic bearing force bandwidth and the stall control authority required to conduct rotating stall control with tip-clearance actuation. The specific question is: how much shaft motion and magnetic bearing force is required to stabilize rotating stall? To answer this question a simplified rotordynamic design analysis and a unique stochastic estimation and control analysis are conducted.

3.1 Simplified Rotordynamic Design and Analysis

A preliminary design of the magnetic bearing rotor is suggested in Figure 4. The solid shaft in Figure 3 is replaced by a hollow shaft including the magnetic bearing rotor laminations. The shaft is pinned at the rear (journal and thrust fluid film bearings) and coupled to the motor drive train. Typical catcher bearing designs do not contact the shaft during magnetic bearing suspension. However for the proposed stall experiments in the NASA high-speed test facility, a fail-safe suspension system is mandatory. In particular, the compressor blades must be protected from possible blade-tip rubs; destructive impacts must also be avoided in the case of a loss of magnetic levitation. A possible fail-safe solution is to use a spring loaded catcher bearing that is

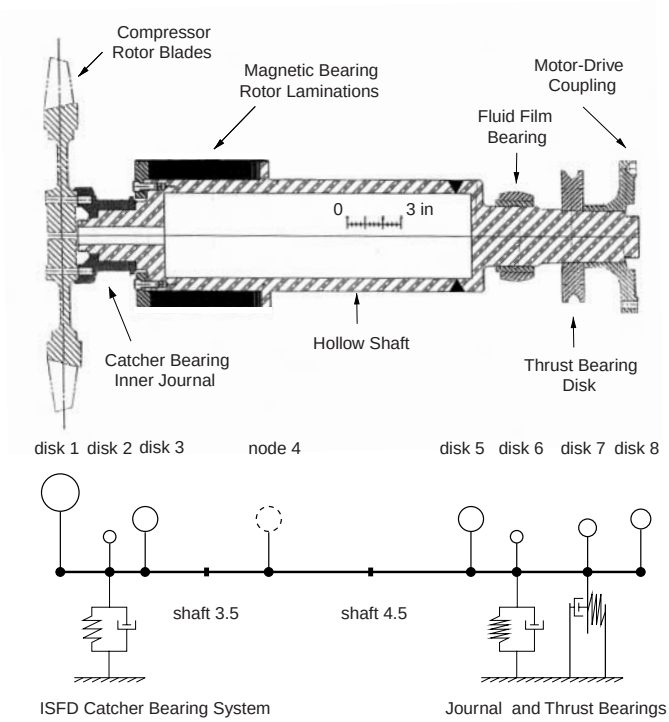

Figure 4. Preliminary magnetic bearing compressor rotor and corresponding lumped parameter model.

always in contact with the shaft. This is the approach adopted for the design analysis.

In the general case of free-free magnetic suspension a simple, single lumped mass analysis is sufficient to obtain a first cut estimate of the required magnetic force. Since in this magnetic bearing application shaft motion is constrained at both ends (soft spring loaded catcher bearing support at the front and conventional fluid film bearings at the rear) the rotordynamic analysis needs to be more detailed.

Therefore in this preliminary design analysis a simple, direct stiffness lumped parameter method (described in Ehrich, 1992) is conducted. The rotor model consists of thin rigid disk elements (lumped masses) connected either by massless flexible beam elements or by flexible uniform shaft elements (distributed mass) as depicted in Figure 4. The overall mass of the shaft is 128.5 kg. Each disk element has four degrees of freedom: two displacement directions normal to the axis of rotation and small angle rotations about the spin axis (precession and nutation). Axial motion is neglected but the fluid film thrust bearing constrains the shaft in angular deflections at the rear and is modeled as an angular spring and an angular damper. The rear journal bearing and the soft spring loaded catcher bearing are modeled as spring and damper elements. For a closed loop analysis[1] the magnetic bearing force can be introduced at node points 3 and 4.

The catcher bearing system for this non-standard high-speed application is suggested to consist of a fluid film journal bearing embedded in a soft spring loaded support. This allows for shaft deflections but still yields a hard stop in case of an emergency. To ensure safe transient operation without large vibrations when critical frequencies are crossed during an emergency shut down, damping must be added in parallel to the soft spring loaded support. One possible, compact solution is an Integral Squeeze Film Damper (ISFD) setup as reported by Santiago et al. (1998). ISFD's are comprised of arcuate squeeze film pads rendering viscoelastic support and wire-EDM webs acting like a squirrel cage.

The open loop whirl speeds, natural frequencies and modeshapes are obtained from an eigenvalue problem resulting from the equations of motion. Assuming that the rotor is spinning at design speed (286 Hz) the first four eigenvalues are plotted in Figure 5 and the modeshapes are reconstructed from the corresponding eigenvectors. The forward whirling modes are marked with pluses and the bearing locations (nodes 2, 6 and 7 in Figure 4) are indicated by the dotted lines. The preliminary hollow shaft design yields two conical modes, denoted as the first and second rigid body modes, which rotate at 0.16 and 0.7 times the rotor frequency, and two flexural modes. The rotation rates of the flexural modes are well above the operating range but note that the first flexural mode is less damped than the second rigid body mode.

[1]Note that the rotor system is open loop stable and that the magnetic bearing is primarily used as a servo-actuator.

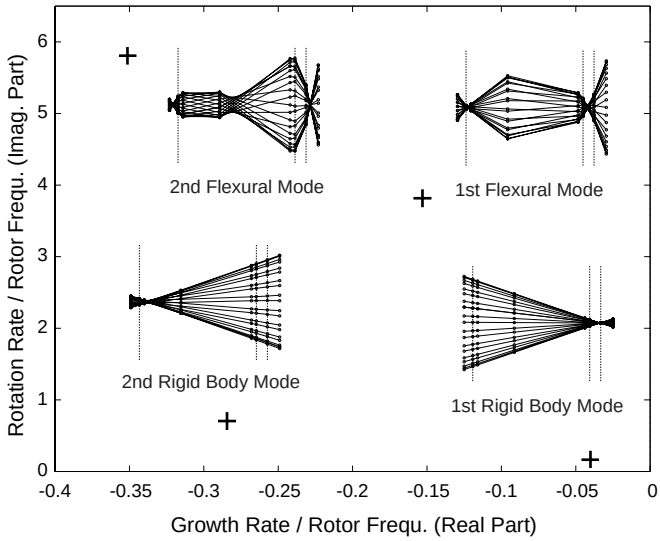

Figure 5. Preliminary open loop rotor model eigenvalues and modeshapes.

This preliminary shaft setup conforms well with the design issues for active tip-clearance control. The magnetic bearing rotor is rigid with a dominant conical rigid body mode at a natural frequency of 0.16 times rotor frequency. The low rotation rate of this first rigid body mode is due to the softly supported catcher bearing system (ISFD). None of the open loop rotordynamic modes are in the vicinity of flow field resonances such as rotating stall, which for this compressor rotates at 0.4 times the rotor frequency. This is a crucial constraint on the rotordynamic design to avoid direct interaction between the compressor prestall dynamics and the structural dynamics. Note that the suggested magnetic bearing rotor yields supercritical operation with respect to the rigid body modes.

In order to obtain an estimate of the required force (introduced by the magnetic bearing) for a certain blade tip deflection, the open-loop transfer function from magnetic bearing force input to blade tip deflection is computed and shown in Figure 6. However, the necessary blade tip deflection for rotating stall control still needs to be determined. This is the key analysis in the preliminary design process and is discussed next.

3.2 Analysis of Tip-Clearance Control Authority

In order to determine the effective shaft motion (i.e. blade tip deflection) for rotating stall control the closed loop system depicted in Figure 7 is considered. The compressor pre-stall dynamics are denoted by the transfer function $\mathbf{G}(s)$. The outputs of $\mathbf{G}(s)$ are the pre-stall pressure perturbations sensed upstream of the rotor $\delta p(t)$, which are fed back to the rotating stall feedback controller $\mathbf{K}(s)$. The controller outputs are the actuator commands $\delta c(t)$, which are modified by the magnetic bearing servo-actuator dynamics $\mathbf{A}_{\mathrm{MB}}(s)$ to yield the actual shaft position and

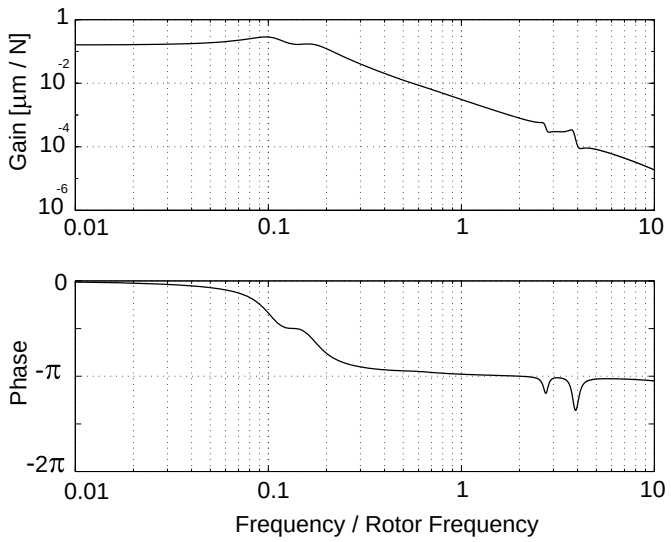

Figure 6. Transfer function from magnetic bearing force input [N] to blade tip deflection [μm].

the corresponding tip-clearance distribution $\delta\varepsilon(t)$. The open loop stable magnetic bearing servo-actuator dynamics $\mathbf{A}_{\mathrm{MB}}(s)$ consist of the shaft rotordynamics and the magnetic bearing servo control loop. The inputs to the compressor pre-stall transfer function $\mathbf{G}(s)$ are the tip-clearance distribution $\delta\varepsilon(t)$ and background noise modeled by unsteady velocity fluctuations $\delta w(t)$. The actuator dynamics $\mathbf{A}_{\mathrm{MB}}(s)$ and the compressor tip-clearance transfer function $\mathbf{G}(s)$ form the plant $\mathbf{P}(s)$, which will be considered in the rotating stall control law design process. Note that this feedback control system is a *regulator* system since the error signal $\delta e(t)$ is composed only of the sensed pressure perturbations. The purpose of the regulator is to drive the pressure perturbations to zero, even if the plant is unstable.

The objective of this analysis is to determine the required closed loop shaft motion $\delta\varepsilon(t)$ to stabilize rotating stall. Since the feedback system is highly resonant and in a noisy environment, the compressor dynamics must be included in the analysis. A stochastic estimation approach is then applied.

Compressor Dynamics with Tip-Clearance Effect. To investigate the effect of blade tip deflection on compressor stability, the compressor pre-stall dynamics $\mathbf{G}(s)$ need to be modeled. Based on the conceptual framework developed by Hynes and Greitzer (1987), Graf et al. (1997) and Gordon (1999) (see Section 1) a two-dimensional, incompressible, state-space compressor model actuated by rotor tip-clearance was created. The derivation of the compressor model equations (see Gordon, 1999) is omitted here and a short model description is given instead.

The overall modeling approach (Moore and Greitzer, 1986) consists of incompressible models of the inlet and exit ducts, the

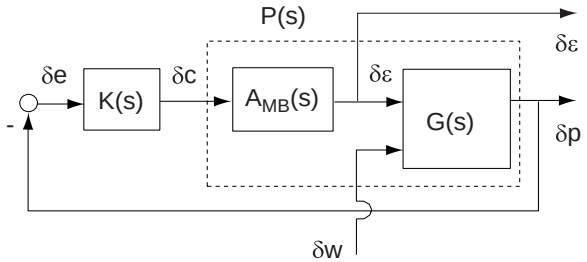

Figure 7. Closed loop magnetic bearing compressor system for stall control.

blade rows, the downstream plenum and throttle. The hub-to-tip ratio is assumed high so that the model is 2-dimensional with axial and circumferential unsteady flow field variations. The rotor and stator blade rows are modeled as semi-actuator disks with unsteady inertia, unsteady deviation and loss terms. The model assumes that the background flow is steady in the reference frame locked to the (rotating) tip-clearance asymmetry so that any tip-clearance distribution (unsteady in the absolute frame) can be prescribed. In a first step the steady, fully non-linear flow field equations are solved in the asymmetry frame to obtain the non-uniform background flow (Hynes and Greitzer, 1987). In a second step a linearized version of the model equations is solved to obtain the behavior of unsteady, small amplitude perturbations to the known steady state non-uniform flow field. Assigning control inputs and outputs to the model and identifying states in the resulting dynamic equations yields a state-space formulation of the compressor model (Gordon, 1999).

The compressor model by Gordon (1999) was modified to include unsteady air injection in addition to tip-clearance actuation. Air injection was used in stall control experiments by Weigl et al. (1998) in the same compressor. This modified compressor model will be useful to match the modeled compressor dynamics to the experimental data by Weigl et al. (1998) and to verify the control authority analysis in a test case for jet injection.

The inputs to the model are the compressor geometry, an axisymmetric tip-clearance compressor characteristic and the sensitivity of the compressor characteristic to changes in axisymmetric tip-clearance. These inputs were based on CFD calculations of the NASA Stage 37 compressor performance. The APNASA blade passage code by Adamczyk et al. (1990) was used to calculate the three-dimensional, viscous flow through the stage for different levels of axisymmetric tip-clearance. In addition, the modeled compressor dynamics were compared to the experimentally obtained system identification results by Weigl et al. (1998). The dynamic model parameters, i.e. loss time lags and system reduced frequency, were adjusted to match the open loop and closed loop compression system poles to the measured eigenvalues. This gives confidence in using the tip-clearance actuated compressor model in the stochastic estimation analysis.

Stochastic Estimation of Closed Loop Shaft Motion. The system input noise $\delta w(t)$ is modeled as white noise of intensity W, which is determined by comparing the spectrum $\Phi_{pp}(\omega)$ of the sensed pre-stall pressure perturbations $\delta p(t)$ obtained from the experiment (Weigl et al., 1998) to the spectrum of the open loop model transfer function $\mathbf{G}(j\omega)$:

$$\Phi_{pp}(\omega) = \mathbf{G}(j\omega)\,\mathbf{G}^T(j\omega)\,W\,. \tag{1}$$

The white noise intensity W is adjusted to match both the peak and the RMS values of the measured and modeled spectra for a compressor operating point that is close to stall. This is shown in Figure 8. Note that the compression system is highly resonant

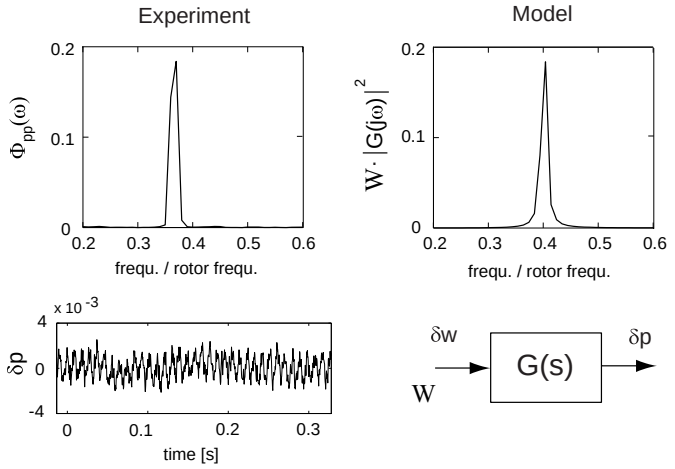

Figure 8. Spectral analysis of open loop pre-stall pressure perturbations (experiment by Weigl et al., 1998) and of open loop compressor model.

and exhibits a sharp peak in the spectrum at a frequency of about 0.4 times the rotor frequency. This resonance of the flow field corresponds to a rotating stall precursor.

A closed loop analysis is conducted next. The circumferentially sensed pressure perturbations are decomposed into circumferential spatial Fourier harmonics. The pre-stall mode with first harmonic circumferential structure is linearly controllable with tip-clearance actuation (if the rotor is off-set from its casing a first harmonic tip-clearance distribution is induced) and all other harmonics are linearly uncontrollable. To simplify the analysis only first harmonic linear control with tip-clearance actuation is considered here. Additional unsteady injection is implemented in this case to stabilize the zeroth harmonic (surge-like) mode. In general non-linear control laws can be used to stabilize the zeroth and second harmonic modes with tip-clearance actuation as discussed in Wang et al. (1999). Such control schemes however will yield further bandwidth and magnetic force requirements.

A simple constant gain control strategy is implemented for $\mathbf{K}(s)$ to stabilize the compressor dynamics. The idea behind constant gain control is as follows. The sensed spatial harmonic waves of the pressure perturbations $\delta p(t)$ are rotated by an optimized angle and multiplied by a constant gain to form the spatial harmonics of the control signal. The commanded shaft position $\delta c(t)$ is modified by the magnetic bearing servo actuator dynamics $\mathbf{A}_{\mathrm{MB}}(s)$ to yield the effective shaft position and tip-clearance distribution $\delta\varepsilon(t)$. In this analysis a simple PI-lead network is used in the inner servo control loop of the magnetic bearing actuator. The constant gain stall controller was tuned to stabilize the zeroth harmonic mode with unsteady air injection and the first harmonic mode with tip-clearance actuation. The mass flow through the compressor is gradually decreased in the simulation until the second harmonic mode becomes unstable. This is shown in Figure 9. Note that it is this mode that determines the overall compressor stability and the compressor operating range.

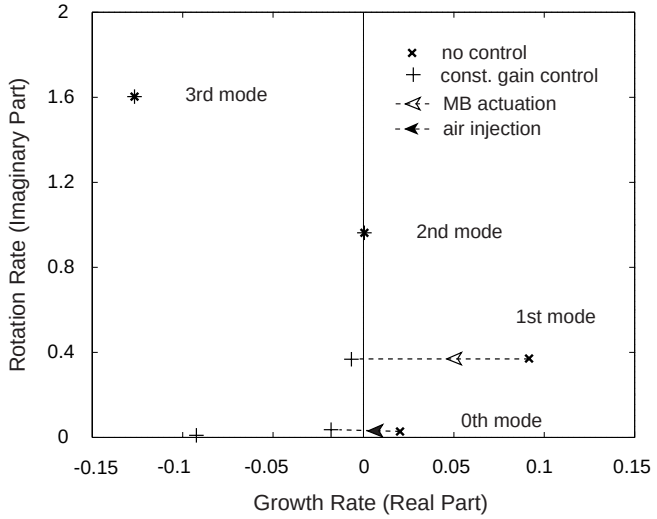

Figure 9. Open loop compressor dynamics (x) and closed loop poles with constant gain control (+).

Defining the state-space matrices $\mathbf{A}_c, \mathbf{B}_c$ and $\mathbf{C}_c$ the time invariant closed loop system in Figure 7 is cast into state-space form

$$\begin{aligned} \dot{\mathbf{x}}(t) &= \mathbf{A}_c \cdot \mathbf{x}(t) \;+\; \mathbf{B}_c \cdot \delta w(t) \\ \delta\varepsilon(t) &= \mathbf{C}_c \cdot \mathbf{x}(t)\,, \end{aligned} \tag{2}$$

where the same system input noise $\delta w(t)$ of intensity W is assumed during stall control. The system output of interest is $\delta\varepsilon(t)$. The RMS of *effective* shaft motion, which is required to stabilize

the compression system, can be estimated from the steady state output covariance $\Sigma_\varepsilon = \mathrm{E}\{\delta\varepsilon(t)^2\}$, where the expected mean of $\delta\varepsilon(t)$ is zero ($\mathrm{E}\{\delta\varepsilon(t)\} = 0$) and $\mathrm{E}\{\}$ denotes the time average of an ergodic process. Assuming steady state, the state covariance Σ_x is obtained from the Lyapunov equation

$$0 = \mathbf{A}_c \, \Sigma_x + \Sigma_x \, \mathbf{A}_c^T + \mathbf{B}_c \, \mathbf{W} \, \mathbf{B}_c^T \, , \tag{3}$$

where $\mathbf{W}$ is the white noise intensity matrix. The output covariance and the RMS of $\delta\varepsilon(t)$ then yield

$$\mathrm{RMS}(\delta\varepsilon) = \sqrt{\Sigma_\varepsilon} = \sqrt{\mathbf{C}_c \, \Sigma_x \, \mathbf{C}_c^T} \, . \tag{4}$$

This procedure is applicable to any actuation scheme and is implemented in a test case for unsteady air injection. The estimated RMS of injector valve motion of $0.141 \; (\pm 0.005)$ compares well to the RMS of the measured actual valve motion of 0.121 in the NASA Glenn stall control experiment, where the valve command ranges from 0 (valve half open) to 1 (valve fully open). This gives confidence in using the presented technique to estimate the effective shaft motion for tip-clearance actuation. The analysis predicts

$$\mathrm{RMS}(\delta\varepsilon) = 207.5 \; (\pm 5.0) \;\; \mu\mathrm{m} \, .$$

The indicated uncertainty in the prediction is due to the uncertainty in the data matched white noise intensity W.

The constant gain control law commands shaft whirl at a frequency of 0.4 times the rotor frequency. This corresponds to the rotation rate of the first harmonic rotating stall precursor. To guarantee a robust magnetic bearing design the required force bandwidth is determined for a shaft displacement of 250 μm for frequencies up to 0.5 times rotor frequency. Using Figure 6 the required magnetic bearing force yields 25kN for frequencies up to 0.5 times rotor frequency (143 Hz). This high load capacity is due to the large mass of the shaft (128.5 kg), the high whirl speed (143 Hz) and radius (250 μm), and the rotordynamic constraints of the shaft at the front end (catcher bearing) and at the rear end (motor drive coupling). Analyzing a typical 5-axis magnetic bearing would result in different requirements, but could use the exact procedure described here.

4 DESIGN REQUIREMENTS

The magnetic bearing servo-actuator design requirements from the preliminary analysis are summarized here. The concept of rotating stall control with tip-clearance actuation requires a magnetic bearing servo-actuator design with state of the art performance and very high load capacities. The desired design and performance requirements include

– rotordynamically stable shaft operation over the entire compressor speed range (0 to 286 Hz).

– maximum shaft deflection of 250 μm to avoid blade tip rubs.

– 250 μm whirl radius between 0 Hz and 143 Hz excitation frequency.

– desired minimum whirl radius of 75 μm at the maximum excitation frequency of 286 Hz.

– maximum bearing diameter of 0.356 m to fit into the compressor hub housing (see Figure 3) without modification of the compressor gas path.

The next section discusses these design issues and presents the detailed design of the magnetic bearing servo-actuator.

5 MAGNETIC BEARING SERVO-ACTUATOR DESIGN

Standard magnetic bearing suspension devices usually only yield large forces during static shaft levitation. The magnetic bearing servo-actuator for active stall control however must deliver a large *dynamic* load capacity and high magnetic forces must be generated over an air gap substantially larger than the nominal gap, since the rotor is whirling off-set from its centerline. In addition, the outer bearing diameter and the space within the compressor hub housing are limited in this application. Hence a special magnetic pole configuration and a new soft magnetic material with relatively small magnetic losses and very high saturation flux densities was considered. Apart from the magnetic bearing actuator itself, the above issues will also strongly influence the actuator power electronics design. It has to be mentioned that, since the magnetic bearing actuator system design is a highly iterative process, only the final results are discussed here.

5.1 Electro-Magnetic Actuator Analysis

Pole Configuration. In order to achieve as much dynamic load capacity as possible within the given compressor housing envelope a non-standard 16 pole configuration is considered. This allows one to pack the required amount of copper wiring within the narrow space between the inner and outer stator diameter. Also, a rather unconventional alternating N-S-N-S pole configuration is used here with the advantage that the magnetic flux through the rotor laminations and the stator back iron is half the value of a standard N-S-S-N pole configuration [2]. Therefore to obtain the same magnetic flux density as delivered by a standard configuration, the stator back iron and rotor lamination radial width can be reduced by a factor of two. This yields a lighter weight magnetic rotor with beneficial influence on the

[2] Usually N-S-S-N pole configurations are considered when high magnetic force capacities are required.

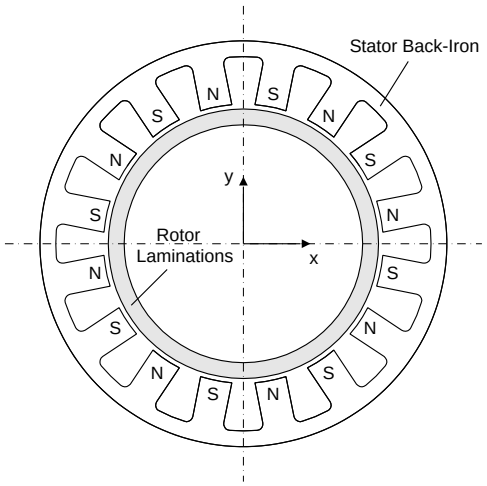

Figure 10. Pole configuration and rotor lamination of magnetic bearing servo-actuator.

overall rotordynamics, bending mode frequencies and achievable whirl radii. However the eddy current and hysteresis losses will be higher than in the standard case since the magnetic flux reversal frequency is doubled. It is clear that in general a trade-off between overall rotor weight and size and rotor heat loss must be made. In the presented application higher priority is attributed to the achievable whirl radii. Figure 10 illustrates the 16 pole N-S-N-S pole configuration and the rotor lamination of the magnetic bearing servo-actuator. The stator and rotor dimensions are given in Table 1.

Servo-Actuator Load Capacity Calculation. The load capacity calculation is based on a full 16 pole flux network model which includes all magnetic interactions and nonlinearities resulting from the magnetization curve of the soft magnetic material. Individual rotor and stator magnetic path geometries are also taken into account but the stray flux between the magnetic poles is neglected. One major advantage of the flux network model compared to finite element modeling techniques is its numerical effectiveness while yielding about the same accuracy (Schmidt et al., 1996). The load capacity calculation mainly depends on the geometry, the air gap and the maximum flux density of the soft magnetic iron. Furthermore, a very important and sometimes limiting factor in the design is the ability of the magnetic bearing servo-actuator to dissipate the heat which is generated from coil, eddy current and hysteresis losses. Therefore an optimal actuator design yields a well balanced trade-off between available copper volume, pole width and actuator surface area which is necessary to conduct the generated heat loss to a heat sink. The final results of the iterative design process are shown in Table 1. Note that the maximum achievable force at the nominal air gap (zero shaft off-set) is approximately 20% higher than the estimated requirement of 25 kN. This is due to the fact that *in the case of a whirling shaft the air gap is increased and a larger force is needed for the same shaft displacement.*

Actuator Dimensions		
Number of Poles	16	-
Inner Actuator Dia.	220	mm
Outer Actuator Dia.	320	mm
Actuator Length	175	mm
Pole Width	24.4	mm
Nominal Air Gap	600	μm
Electro-Magnetic Properties		
Saturation Flux Density (Co Iron)	2.4	Ts
Max. Force (at nom. air gap)	31.6	kN
Flux Density (at max. force)	2.28	Ts
Current Stiffness (K_i)	1.021	kN/A
Position Stiffness (K_x)	93.149	kN/mm
Max. Current (Saturation)	100	A
Max. Voltage (Saturation)	300	V
Electric Resistance	37	mΩ
Coil Inductance	6.9	mH

Table 1. Optimized magnetic bearing servo-actuator design parameters.

5.2 Overall Dynamic System Analysis - Achievable Whirl Radii

In order to compute the achievable whirl radii the magnetic bearing servo-actuator model must be combined with a rotordynamic model of the compressor shaft. Since large forces are generated at high frequencies, non-linear current effects and voltage saturation of the electric power amplifier must also be taken into account. These models are briefly outlined here.

Rotordynamic Model. A standard finite element modeling approach is carried out to obtain a system of differential equations describing the rotor motion. This approach accounts for shear force influence, gyroscopic effects and additional lumped mass and rotational inertia effects:

$$\mathbf{M}\,\ddot{\mathbf{z}} + (\mathbf{G}+\mathbf{D})\,\dot{\mathbf{z}} + \mathbf{K}\,\mathbf{z} = \mathbf{B}_{\text{act}}\,\mathbf{f}_{\text{act}}\,, \tag{5}$$

where $\mathbf{z}$ is the rotor position vector, containing both the horizontal and the vertical displacements x and y of the elements.

M denotes the mass matrix and includes all inertia properties (mass, radial moments of inertia). The **G** matrix contains the gyroscopic terms (polar and radial moments of inertia, rotational speed). The radial and axial fluid film bearings at the motor coupling end and the ISFD catcher bearing system at the compressor wheel end are modeled as spring-damper elements and are included in the stiffness matrix **K** and the damping matrix **D**. The actuator force $\mathbf{f}_{\text{act}}$ is coupled into the rotordynamic system by the influence matrix $\mathbf{B}_{\text{act}}$ which defines the geometric point of action of the magnetic force. The homogeneous solution of Equation (5) can be analyzed in terms of a Campbell diagram which is shown in Figure 11. The two rigid body forward and backward whirling modes are crossed by the one-per-rev line (1-E) at about 30 Hz, 180 Hz and 200 Hz. Note that none of the flexural modes are crossed despite the strong gyroscopic effects and that the rigid body mode frequencies compare well to the preliminary results (see Figure 5) obtained from the simple lumped parameter model. The frequencies of the two rigid body modes mostly depend on the stiffness of the fluid film and catcher bearings, the mass properties of the compressor shaft and the actuator feedback control. In order to limit the vibration level when the rigid body critical frequencies are crossed, the rotor must either be well balanced or the bearings, especially the magnetic actuator, must dissipate a substantial amount of energy, i.e. provide a sufficient amount of external damping to the system.

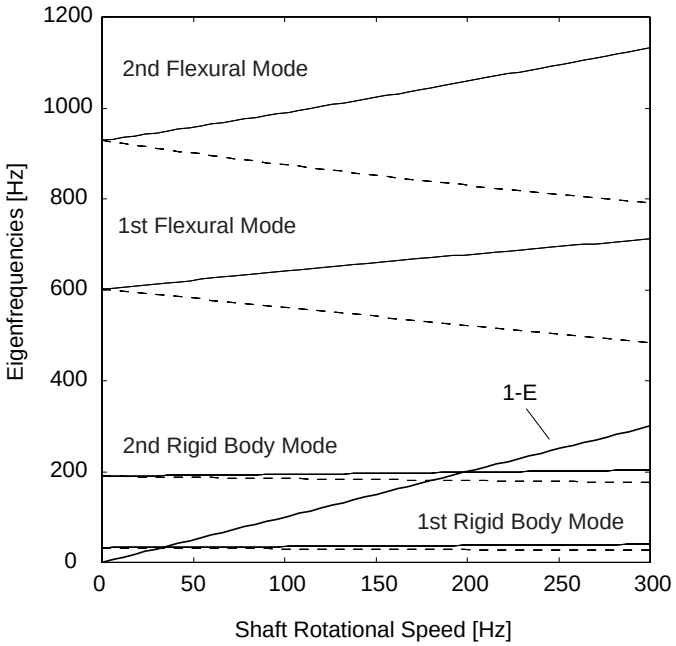

Figure 11. Campbell diagram of magnetic bearing servo-actuator (forward and backward whirling modes are marked solid and dashed respectively).

Actuator and Power Amplifier Model. A linearized model of the magnetic bearing servo-actuator is used to keep the computation times at an affordable level. Non-linear effects are included in the voltage and current saturation characteristics of the power amplifier. The linearized actuator force can be written as

$$\mathbf{f}_{\text{act}} = \mathbf{K}_x\, \mathbf{z}_b + \mathbf{K}_i\, \mathbf{i}\,, \tag{6}$$

where matrix $\mathbf{K}_x$ contains the two identical position stiffnesses in the x and y directions and $\mathbf{K}_i$ contains the corresponding current stiffnesses of the magnetic bearing servo-actuator. Vectors $\mathbf{z}_b$ and $\mathbf{i}$ denote the rotor position within the magnetic actuator and the control current input respectively. In order to combine Equations (5) and (6) $\mathbf{z}_b$ must be transformed into $\mathbf{z}$ assuming rigid body relations between the shaft locations. The amplifier dynamics contain the influence of the actuator inductance and resistance **L** and **R** and the back-EMF term due to rotor motion (for details see Vischer and Bleuler, 1990):

$$\mathbf{u} = \mathbf{R}\,\mathbf{i} + \mathbf{L}\frac{d\mathbf{i}}{dt} + \frac{1}{2}\mathbf{K}_i^T\, \dot{\mathbf{z}}_b\,, \tag{7}$$

where vector **u** contains the coil voltages. The achievable whirl radii can now be determined by solving Equations (5), (6) and (7) for position vector **z**.

The resulting high order system of non-linear differential equations must be solved numerically and the solution procedure is quite involved and time consuming. Instead a much faster iterative solution procedure was developed. First let us consider the following thought experiment: if the whirling rotor was a single lumped mass then it is kept in orbit by a single radial force of constant amplitude with a phase of 180 degrees relative to the displacement vector. Therefore in the iterative solution procedure the excitation force is assumed to be 180 degrees out of phase despite gyroscopic effects of the rotor and external stiffnesses and damping properties of the fluid film journal bearings[3]. It has to be mentioned that in the experiment the same effect can be achieved by introducing a synchronous signal rejection scheme in the magnetic bearing feedback controller (for details see Herzog et al., 1996). This yields a completely force-free rotation about the principal axis of the rotor and eliminates the transmission of synchronous unbalance forces to the machine housing. Also since the steady-state whirl orbits are of interest all transient parts of the solution are neglected and Equations (5), (6) and (7) are solved in the frequency domain.

The results of the iterative solution procedure are shown in Figure 12 for the shaft spinning at design speed (286 Hz). The plot on the left hand side depicts the family of non-linear current-force characteristics of the magnetic bearing servo-actuator and

[3]It can be shown that this assumption yields a maximum error in the phase of about 20 degrees for frequencies above 50 Hz.

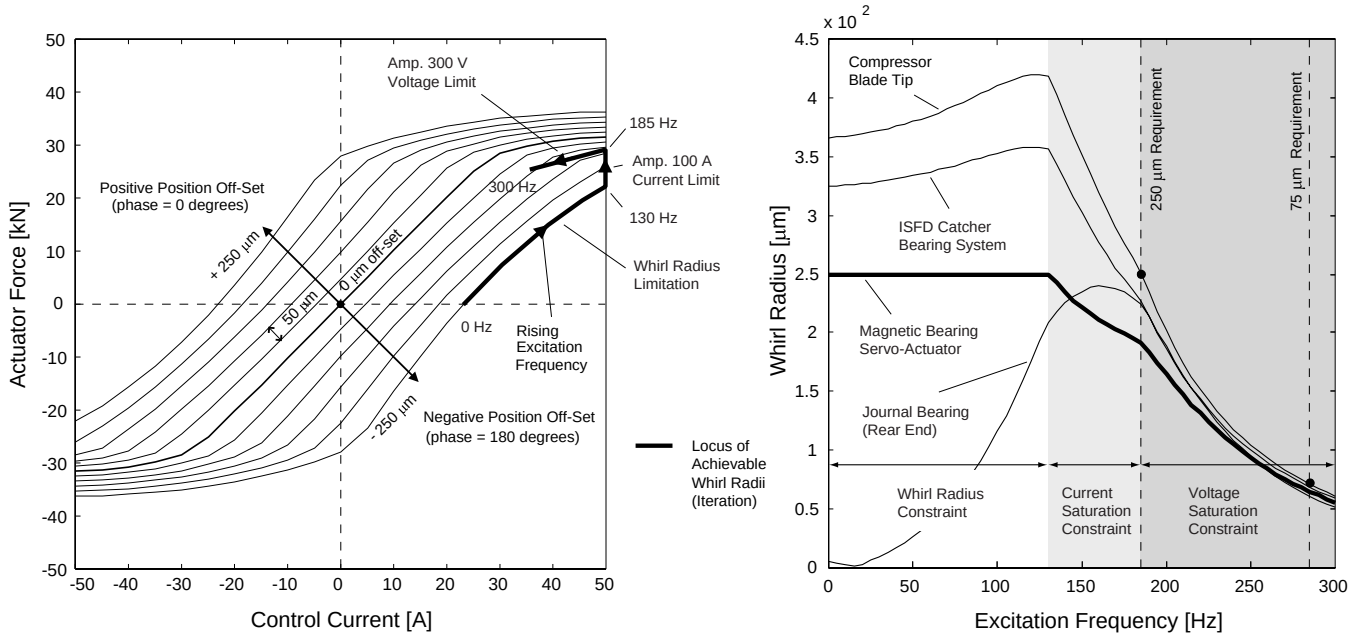

Figure 12. Current-force characteristic of magnetic bearing servo-actuator and operating locus (left); achievable whirl radii at several shaft locations and amplifier operation limits (right).

the locus of operating points ranging from 0 to 300 Hz excitation frequency at maximum available power (thick solid line). Note that the effect of a varying air gap is included in the calculation. The achievable whirl radii at several shaft locations are plotted on the right hand side together with the operational constraints of the amplifier (300V saturation voltage, 100 A saturation current split into 50 A bias and 50 A maximum control current) and the whirl radius limitation at the magnetic bearing location (250 μm). The results show that the design requirements stated in Section 4 are fulfilled: 250 μm compressor blade tip deflection is achieved up to 185 Hz (the blade tip displacement in this frequency band is even higher than the requirement since the actuator is operating at maximum available power) and a minimum of 75 μm is obtained at the synchronous excitation frequency of 286 Hz. The nonlinear current and voltage saturation effects of the amplifier are well visible in these performance characteristics.

5.3 Heat Loss and Cooling Analysis

As mentioned earlier, a trade-off between achievable whirl radii and magnetic bearing heat loss had to be considered in this design. Since the required shaft displacements and excitation frequencies are rather high compared to standard magnetic bearing applications the heat loss is expected to be substantial. Therefore a detailed heat loss and cooling analysis described in Traxler (1985) was carried out. The analysis involved the modeling of magnetic bearing stator losses (coil resistance, magnetic reversal (hysteresis) and eddy current loss), magnetic bearing rotor lamination losses (hysteresis and eddy current loss), aerodynamic windage loss in the magnetic bearing gap and dissipation in the fluid film journal and catcher bearing systems due to high frequency rotor whirl. All magnetic bearing stator loss and the dissipation in the fluid film journal bearings must be supplied by the power amplifiers. The lamination and aerodynamic losses in the magnetic bearing rotor however must be supplied by the motor drive. The results of the heat loss analysis are summarized in Table 2. It should be mentioned that these values correspond to a worst-case situation since all losses are taken at their peak values (different frequencies in Table 2) and the shaft is assumed to be spinning at design speed (286 Hz).

The cooling concept for the NASA Stage 37 magnetic bearing axial flow compressor includes three different cooling systems and a preliminary cooling analysis was also conducted. Water cooling through a cooling jacket around the stator is estimated to provide a cooling power of 950 W which covers the stator losses plus a part of the aerodynamic losses. Cooling oil is run through and around the fluid film bearings at the front and rear shaft end and is expected to exchange a total of 8650 W power due to the bearing dissipation and rotor lamination loss. In addition cold high pressure air is run around the shaft with an estimated cooling power of 2280 W to cover most of the aerodynamic losses. Clearly this analysis indicates that heat dissipation significantly complicates this particular magnetic bearing design.

Stator Losses	[W]	Frequency [Hz]
Coil Resistance	560	115
Eddy Current & Hysteresis	180	190
Rotor Losses		
Windage Loss	2500	286
Eddy Current & Hysteresis	5060	286
Bearing Dissipation		
ISFD Catcher Bearing	864	120
Fluid Journal Bearing	2729	185

Table 2. Total mechanical, electro-magnetic and aerodynamic losses at design speed (286 Hz).

6 CLOSED LOOP STALL CONTROL SIMULATION

The final design of the magnetic bearing servo-actuator was then used to simulate the closed loop stall control experiment. The final magnetic bearing system dynamics $\mathbf{A}_{\mathrm{MB}}$ were included in the closed loop system shown in Figure 7. As mentioned earlier, a simple PI-lead network was implemented in the inner servo control loop of the magnetic bearing actuator. Again a constant gain stall controller was used in the outer loop to stabilize the zeroth harmonic mode with unsteady air injection and the first harmonic mode with tip-clearance actuation. The compressor was throttled into stall and a 2.3% reduction of stalling mass flow was obtained.

The stable operating range extension with tip-clearance actuation is comparable to the results obtained in the same compressor by Weigl et al. (1998) using unsteady air injection. These results show that tip-clearance actuation with magnetic bearings is an effective actuation scheme and establish the viability of magnetic bearings for stall control in high-speed compressors.

7 SUMMARY AND CONCLUDING REMARKS

This paper presents a general design procedure to develop magnetic bearing servo-actuators for high-speed compressor stall control. The design procedure is carried out in an example analysis for the NASA Glenn high-speed single stage axial flow compressor and results specific to this compressor are reported in this paper. It has to be pointed out that this specific application introduced special design constraints and unusual complexities due to the existing test rig setup and environment. For example, the constraint of a two-axis magnetic bearing with a contacting catcher bearing system and an existing fluid film journal bearing setup at the motor drive coupling end are not encountered in a general design problem. If a compressor with magnetic bearings were developed from scratch, many of the design constraints would be relaxed. Therefore the design process is emphasized here rather than the presented numbers.

The key analysis in the design process is to determine the control authority of tip-clearance actuation and the design requirements of the magnetic bearing. A unique stochastic estimation and control analysis is presented and applied first to unsteady air-injection actuation as a test case. The obtained results compare well to experimental data and give confidence in using this procedure for tip-clearance actuation.

Next the magnetic bearing servo-actuator design requirements are determined by combining the stochastic estimation and control approach with a preliminary rotordynamic analysis and a dynamic compressor tip-clearance model which utilizes both CFD and experimental data. Although the results are for a specific experimental rig, they indicate that in general the concept of rotating stall control with tip-clearance actuation requires a magnetic bearing servo-actuator design with state of the art performance and very high dynamic load capacities.

A detailed electro-magnetic and mechanical analysis of the magnetic bearing servo-actuator is conducted and the design fulfills the requirements. The magnetic bearing servo-actuator yields a remarkably high dynamic force level and bandwidth which are necessary for this application due to the large mass and the high excitation frequencies. The design considers a trade-off between the achievable whirl radii and the generated heat loss. The heat loss calculation reveals rather high values due to the special constraints and in addition a cooling analysis is conducted. Active water, oil and air cooling are considered necessary to provide sufficient cooling power.

Stall control laws are then developed and the final magnetic bearing servo-actuator design is implemented in a closed loop stall control simulation to determine the benefit in stable compressor operating range. The simulation results yield a 2.3% reduction in stalling mass flow which is comparable to results with unsteady air injection. The design and simulation results presented in this paper establish the viability of magnetic bearings for stall control in aero-engine high-speed compressors.

ACKNOWLEDGMENTS

This research was conducted under collaboration between the Gas Turbine Laboratory at MIT, the NASA Glenn Research Center and MECOS Traxler AG. The authors would like to thank Dr. A. Strazisar, Dr. G. Brown and Dr. A. Kascak at the NASA Glenn Research Center, Dr. K. Gordon and Dr. F. Ehrich at MIT, Dr. L. San Andrés and Dr. A. Palazzolo at Texas A&M University for their support and insightful discussions. This project was conducted under NASA grant NAG3-1457.

REFERENCES

Adamczyk J., Celestina M., Beach T., and Barnett M., 1990. "Simulation of Three-Dimensional Viscous Flow Within a Multistage Turbine." *ASME J. of Turbomachinary*, vol. 112 pp. 370–376.

Ehrich F., 1992. *Handbook of Rotordynamics*. McGraw-Hill Book Company.

Epstein A., Williams J., and Greitzer E., 1989. "Active Suppression of Aerodynamics Instabilities in Turbomachines." *J. of Propulsion*, vol. 5, 2 pp. 204–211.

Gordon K., 1999. *Three-Dimensional Rotating Stall Inception and Effects of Rotating Tip Clearance Asymmetry in Axial Compressors*. Ph.D. thesis, Department of Aeronautics and Astronautics, MIT.

Graf M., Wong T., Greitzer E., Marble F., Tan C., Shin H.W., and Wisler D., 1997. "Effects of Non-Axisymmetric Tip Clearance on Axial Compressor Performance and Stability." In *ASME Gas Turbine and Aeroengine Congress and Exposition, Orlando, FL, Paper 97-GT-406*.

Herzog R., Bühler P., Gähler C., and Larsonneur R., 1996. "Unbalance Compensation Using Generalized Notch Filters in the Multivariable Feedback of Magnetic Bearings." *IEEE Transactions on Control Systems Technology*, vol. 4 pp. 580–586.

Hynes T. and Greitzer E., 1987. "A method for assessing Effects of Circumferential Flow Distortion on Compressor Stability." *ASME J. of Turbomachinary*, vol. 109 pp. 371–379.

Moore F. and Greitzer E., 1986. "A Theory of Post-Stall Transients in Axial Compressors: Part I — Development of the Equations." *ASME J. of Engineering for Gas Turbines and Power*, vol. 108 pp. 68–76.

Reid L. and Moore D., 1978a. "Design and Overall Performance of Four Highly Loaded, High Speed Inlet Stages for and Advanced High Pressure Ratio Core Compressor." Tech. Rep. TP-1337, NASA.

Reid L. and Moore D., 1978b. "Performance of Single-Stage Axial-Flow Transonic Compressor With Rotor and Stator Aspect Ratios of 1.19 and 1.26, Respectively, and With Design Pressure Ratio 1.82." Tech. Rep. TP-1338, NASA.

Santiago O., San Andrés L., and Olivera J., 1998. "Imbalance Response of a Rotor Supported on Open-End Integral Squeeze Film Dampers." In *ASME Gas Turbine and Aeroengine Congress and Exposition, Stockholm, Sweden, Paper 98-GT-6*.

Schmidt E., Platter T., and Springer H., 1996. "Force and Stiffness Calculations in Magnetic Bearings - Comparison Between Finite Element Method and Network Theory." In *5th International Symposium on Magnetic Bearings, Kanazawa, Japan*. (pp. 259–264).

Traxler A., 1985. *Eigenschaften und Auslegung von berührungsfreien elektromagnetischen Lagern*. Ph.D. thesis, Swiss Federal Institute of Technology, ETH Zürich. ETH thesis No. 7851.

Vischer D. and Bleuler H., 1990. "A New Approach to Sensorless and Voltage Controlled AMB's Based on Network Theory Concepts." In *2nd International Symposium on Magnetic Bearings, T. Higuchi (ed.) University of Tokyo*.

Wang Y., Paduano J., and Murray R., 1999. "Nonlinear Control Design for Rotating Stall and Surge With Tip Clearance Actuation." In *IEEE International Conference on Control Applications*.

Weigl H., Paduano J., Fréchette L., Epstein A., and Greitzer E., 1998. "Active Stabilization of Rotating Stall and Surge in a Transonic Single Stage Axial Compressor." *ASME J. of Turbomachinary*, vol. 120 pp. 625–636.